arXiv:2501.11860v1 [cs.IT] 21 Jan 2025

Bayesian Despeckling of Structured Sources

Ali Zafari*, Shirin Jalali*

Abstract

Speckle noise is a fundamental challenge in coherent imaging systems, significantly degrading image quality. Over the past decades, numerous despeckling algorithms have been developed for applications such as Synthetic Aperture Radar (SAR) and digital holography. In this paper, we aim to establish a theoretically grounded approach to despeckling. We propose a method applicable to general structured stationary stochastic sources. We demonstrate the effectiveness of the proposed method on piecewise constant sources. Additionally, we theoretically derive a lower bound on the despeckling performance for such sources. The proposed depseckler applied to the 1-Markov structured sources achieves better reconstruction performance with no strong simplification of the ground truth signal model or speckle noise.

1 Introduction

1.1 Problem statement

Multiplicative noise, commonly referred to as *speckle* noise, poses a significant challenge in coherent imaging systems such as synthetic aperture radar [1], optical coherence tomography [2], and digital holography [3]. The inherent non-linearity of the multiplicative noise model complicates the analysis and design of optimal despeckling algorithms—denoising methods tailored to address multiplicative noise and recover the underlying signal—even for relatively simple structured sources [4].

Mathematically, the despeckling problem can be formulated as follows. Consider a stationary stochastic process $\mathbf{X} = \{X_i\}_{i\in\mathbb{N}}$, $X_i \in \mathcal{X}$, observed under a *multiplicative noise model*, $Y_i = X_i W_i$, where W_i represents the speckle noise. In most coherent imaging applications, the speckle noise process is assumed to be fully developed and is therefore modeled as Gaussian [5]. Here, we assume that $\{W_i\}_i$ are independent and identically distributed as standard normal random variables, $\mathcal{N}(0,1)$. The despeckling (or denoising under speckle noise model) goal is to recover X^n from speckle-corrupted measurements Y^n.

In a Bayesian framework, given the source distribution $p(x^n)$, the optimal MMSE despeckler lets $\hat{X}^n = \mathrm{E}[X^n|Y^n]$. However, even for additive noise, direct computation of $\mathrm{E}[X^n|Y^n]$ is often intractable and highly challenging. Additionally, the source distribution $p(x^n)$ is rarely accessible in practice, and typically, only samples from this distribution are available. These challenges raise a fundamental question:
Question. Can we design a theoretically founded, computationally efficient framework for despeckling that applies to a broad class of structured sources?

1.2 Related work

Theoretically derived Bayesian despeckling methods can be broadly categorized into two approaches: adaptive linear minimum mean squared error (MMSE) filtering and maximum a posteriori (MAP) estimation [1,4]. In early work, [6] proposed an affine approximation to the nonlinear speckle model, minimizing the ℓ_2 norm

*Rutgers University, New Brunswick, Department of Electrical and Computer Engineering (ali.zafari@rutgers.edu, shirin.jalali@rutgers.edu).

and matching first-order moments to derive the MMSE estimator. A fully driven linear MMSE approach was later introduced in [7], avoiding the approximation errors of the affine model. Both methods rely on local statistics calculated over pre-defined windows, yielding comparable despeckling performance in practice [8]. A refinement for images was proposed in [9], leveraging the local gradient to adaptively redefine neighborhoods for improved statistical estimation.

Beyond linear MMSE methods, MAP estimators have been extensively studied, often requiring strong assumptions about the signal prior distribution. For example, [10] considered a MAP framework with a gamma prior, in contrast to the Gaussian prior used in [11]. These methods generally assume local stationarity of the signal and parameterize its distribution using moments computed within a local window.

Other approaches explore regularization-based techniques, such as total variation (TV) minimization [12]. For speckle noise, [13] combines a gamma likelihood fidelity term with the TV regularizer, though the inherent nonconvexity of the speckle model limits its practical utility. A log-transform-based linearization of the speckle model was proposed in [14], where the additive noise is denoised and rescaled back by exponentiation. However, this approach suffers from degraded performance due to mismatches between the log and signal domains.

Additionally, drawing inspiration from denoising methods designed for additive noise, various heuristic despeckling approaches—such as non-local means [15], SAR-BM3D [16], and neural network-based solutions [17]—have been widely adopted, particularly for high-resolution imaging tasks. For instance, the DnCNN architecture [18] has been trained for despeckling images, both with the log-transformation [19] and without it [20]. Also, self-supervised despeckling algorithms, based on the Noise2Noise [21] and Noise2Void [22] frameworks originally developed for additive denoising, are extended to the despeckling problem in [23] and [24], respectively. State-of-the-art generative models have also been explored for addressing the image despeckling problem. These include the use of generative adversarial networks as demonstrated in [25] and diffusion-based probabilistic models as explored in [26].

1.3 Our contribution

We propose Bayesian Despeckling via QMAP (BD-QMAP), a novel despeckling algorithm inspired by the Quantized Maximum a Posteriori (Q-MAP) estimator [27], originally developed for additive noise. QMAP defines the estimator as the minimizer of a cost function over the space of all possible solutions within the signal's support space $\mathcal{X}^n$. The cost function consists of two terms: a negative log-likelihood term capturing the noise model and a regularization term enforcing distributional similarity between the quantized reconstruction and quantized ground-truth data. By leveraging learned statistics, QMAP assigns weights to unique realizations of the reconstruction, effectively reducing the impact of irrelevant solutions.

Building on these ideas, BD-QMAP adapts QMAP principles to multiplicative noise, tailoring the framework for general structured sources. To clarify its operation, we simplify the formulation for classic structured sources, including memoryless sources with a mixture of continuous and discrete components and piecewise-constant sources. We establish a theoretical lower bound on BD-QMAP's performance for piecewise-constant first-order Markov processes. Experimental results demonstrate that BD-QMAP achieves state-of-the-art performance on piecewise-constant sources modeled as first-order Markov processes.

1.4 Notations and definitions

Finite sets are denoted by calligraphic letters. For a finite set $\mathcal{A}$, $|\mathcal{A}|$ denotes its size. For $b \in \mathbb{N}^+$, the b-bit quantized version of $x \in \mathbb{R}$ is denoted as $[x]_b$, defined as $[x]_b = 2^{-b}\lfloor 2^b x \rfloor$. For $x^k \in \mathcal{X}^k$, $[x^k]_b$ denotes the element-wise b-bit quantization of x^k. The b-bit quantized version of $\mathcal{X} \subset \mathbb{R}$ is denoted by $\mathcal{X}_b$, defined as

$$\mathcal{X}_b = \{[x]_b : \ x \in \mathcal{X}\}.$$

Consider sequence $u^n \in \mathcal{U}^n$, with finite alphabet $\mathcal{U}$ ($|\mathcal{U}| < \infty$). The k-th order empirical distribution of u^n,

$\hat{p}^k(\cdot|u^n)$, is defined as follows. For $a^k \in \mathcal{U}^k$,

$$\hat{p}^k(a^k|u^n) = \frac{1}{n-k+1} \sum_{i=1}^{n-k+1} \mathbb{1}_{u_i^{i+k-1}=a^k}. \tag{1}$$

1.5 Paper organization

This paper is organized as follows: Section 2 introduces the BD-QMAP despeckler. Section 3 discusses its application to two classical structured sources and derives a lower bound for the MSE of the piecewise constant source. Section 5 describes numerical experiments, including the algorithm's implementation and a performance comparison with other despeckling methods.

2 Bayesian Despeckling via QMAP

Consider the despeckling problem, where the goal is to recover X^n from noisy measurements $Y^n = X^n W^n$. Here, X^n follows a known prior distribution $p(x^n)$ and W^n is i.i.d. $\mathcal{N}(0, \sigma_w^2)$. In this formulation, we neglect the effect of additive noise, focusing solely on the multiplicative noise model, as is commonly done in coherent imaging applications. Note that under this model, the variance of speckle noise does not play a role, as one can always scale the measurements by $1/\sigma_w$. Therefore, in the remainder of the paper, without loss of generality, we assume that $\sigma_w^2 = 1$.

Inspired by the Q-MAP denoiser, introduced for additive noise [27], we propose BD-QMAP, a novel despeckling algorithm that is applicable to general structured sources. To define this approach, first we review how the structure of the source is accounted for in the original Q-MAP algorithm. For $a^k \in \mathcal{U}_b^k$, define $w_{a^k} > 0$ as

$$w_{a^k} = -\log \mathrm{P}([X^k]_b = a^k),$$

where the probability P is computed with respect to the known distribution $p(x^n)$. Here, $k \in \mathbb{N}^+$ and $b \in \mathbb{N}^+$ denote the memory parameter and the quantization level, respectively. Then, given weights $\mathbf{w} = (w_{a^k} : a^k \in \mathcal{U}_b^k)$, the weight assigned to sequence $u^n \in \mathcal{U}^n$ is defined as

$$c_{\mathbf{w}}(u^n) = \sum_{a^k \in \mathcal{X}_b^k} w_{a^k} \hat{p}^k(a^k|u^n)(a^k|[X^k]_b). \tag{2}$$

Finally, the BD-QMAP method, recovers X^n as $\hat{X}^{n,(k,b)}$ defined as

$$\hat{X}^{n,(k,b)} = \arg\min_{u^n \in \mathcal{X}^n} \frac{1}{n} \sum_{i=1}^{n} \big(\log u_i^2 + \frac{Y_i^2}{u_i^2} \big) + \frac{\lambda}{b} c_{\mathbf{w}}(u^n). \tag{3}$$

The cost function in (3) comprises of two terms. The first term represents a fidelity criterion derived from the negative likelihood of the observations given the signal under the multiplicative noise model. Note that given $X^n = x^n$, $Y^n \sim \mathcal{N}(\mathbf{0}, X^2)$, where $X = \mathrm{Diag}(\mathbf{x})$. Therefore,

$$-\log p(y^n|x^n) = \frac{1}{2} \sum_{i=1}^{n} (\log x_i^2 + \frac{y_i^2}{x_i^2}) + C.$$

where C is a constant not depending on x^n or y^n. The second term in (3) imposes a prior on the ground-truth signal using the set of weights assigned to the quantized representation of the candidate reconstruction. The weights defined in (2) are a function of the signal's known distribution. In other words, the weights are expected to summarize the source's n-dimensional distribution characterized by $p(x^n)$ into a finite number $|\mathcal{X}_b|^k$ of positive weights.

A key advantage of this approach is that it leads to a tractable approach for modeling and utilizing the sources structure. It can be shown that for structured sources, i.e., the sources with information dimension strictly less than one [28, 29], identified by having singularities in their distributions, e.g., spike and slap distribution, the weights $\mathbf{w}$ can be divided into two groups: 1) A small set of weights that identify the key structure of the source, and 2) a large set of weights that have negligible impact in the optimization [27].

Remark 1. *Solving the BD-QMAP optimization is challenging due to the nature of the cost function, which combines a non-convex loss term derived from the log-likelihood and a regularization term defined on the discretized space of sequences. To address this complexity, the optimization can be simplified by restricting the search space to $\mathcal{X}_b^n$, the space of quantized sequences. As explained in Section 5.1, this restriction enables the application of the Viterbi algorithm for efficient optimization. While this approach is suboptimal compared to solving the original problem, it offers significant computational advantages. Moreover, for cases such as the piecewise-constant source studied later, this simplification facilitates learning the structure of the jumps, allowing the original optimization to be solved in the continuous space with improved computational efficiency.*

To gain deeper insight into the BD-QMAP optimization and the roles of its two terms, we examine two classic structured processes in the next section: structured i.i.d. sources and piecewise-constant sources. For each source, we derive a simplified form of the BD-QMAP despeckler optimization. Moreover, for the piecewise-constant source, we theoretically establish a lower bound on the expected mean squared error (MSE) achievable by the BD-QMAP method.

3 Analysis of BD-QMAP for classic structured sources

In the following, we focus on two classic structured source models and study BD-QMAP under each model.

3.1 Structured memoryless source

Consider an i.i.d process $\mathbf{X}$ such that $X_i \sim (1-q_0)\delta_{x_m} + q_0 \text{Uniform}(x_m, x_M)$, Setting $k=1$ and using the results of [27, Sec. 3.1] to simplfy the second term in (3), the BD-QMAP algorithm can be written as

$$\hat{X}^{n,(1,b)} = \arg\min_{u^n \in \mathcal{U}^n} \Big[\frac{1}{n} \sum_{i=1}^{n} \big(\log u_i^2 + \frac{Y_i^2}{u_i^2} \big) + \lambda(1+\gamma)(1 - \hat{p}^1(x_m|[u^n]_b)) \Big],$$

where $\gamma = \frac{1}{b}\log(\frac{1-q_0}{q_0} + 2^{-b}) = O(\frac{1}{b})$. Note that $1 - \hat{p}^1(x_m|[u^n]_b) = \frac{1}{n}\sum_{i=1}^{n} \mathbb{1}_{[u_i]_b \neq x_m}$. Therefore, the optimization simplifies to a symbol-by-symbol optimization as follows:

$$\hat{X}_i^{(1,b)} = \arg\min_{u \in \mathcal{U}} \Big[\log u^2 + \frac{Y_i^2}{u^2} + \lambda(1+\gamma)\mathbb{1}_{[u]_b \neq x_m} \Big].$$

Note that if $[u]_b \neq x_m$, the loss function is minimized at $\hat{x}_i = |Y_i|$. Therefore, assuming that b is large, to solve the optimization one needs to compare $\log Y_i^2 + 1 + \lambda \gtrless \log x_m^2 + \frac{Y_i^2}{x_m^2}$, or

$$1 + \lambda \gtrless (\frac{Y_i}{x_m})^2 - \log(\frac{Y_i}{x_m})^2. \tag{4}$$

This optimization has the following closed-form solution

$$\hat{X}_i^{(1,b)} = |Y_i| \mathbb{1}_{|Y_i|/x_m \notin \mathcal{I}_\lambda} + x_m \mathbb{1}_{|Y_i|/x_m \in \mathcal{I}_\lambda},$$

where $\mathcal{I}_\lambda$ denotes an interval around one that is defined by (4).

3.2 Piecewise constant source

Consider a first order Markov process $\mathbf{X}$ such that given $X_i = x_i$, X_{i+1} is distributed as $(1-q_0)\delta_{x_i} + q_0\text{Uniform}(x_m, x_M)$. Setting $k=2$ and again using the results of [27, Sec. 3.2], the BD-QMAP algorithm simplifies to

$$\hat{X}^{n,(2,b)} = \arg\min_{u^n \in \mathcal{X}^n} \Big[\frac{1}{n}\sum_{i=1}^{n}\big(\log u_i^2 + \frac{Y_i^2}{u_i^2}\big) + (\lambda + \frac{1}{b}\eta)\frac{N_J([u^n]_b)}{n-1}\Big], \tag{5}$$

where $\eta = -\lambda \log q_0 - \log(1-q_0+q_0 2^{-b})$ is a constant not depending on u^n. Here, $N_J(u^n) = |\{i : u_i \neq u_{i+1}\}|$ denotes the number of jumps in u^n.

To provide a clearer understanding of how the BD-QMAP loss function operates, as well as the roles of its two key terms—the first ensuring reconstruction fidelity to the observations, and the second acting as a regularizer to promote the source structure—the following lemma offers an alternative representation of (5).

Lemma 1. *Solving the optimization in* (5) *is equivalent to solving the following optimization*

$$\hat{X}^{n,(2,b)} = \min_{k\in\{0,\dots,n-1\}}\Big(\min_{(n_1,\dots,n_{k+1})}\sum_{j=1}^{k+1} n_j \log\big(\frac{1}{n_j}\sum_{l\in\mathcal{I}_j} Y_l^2\big) + \frac{n}{n-1}(\lambda+\frac{1}{b})k\Big), \tag{6}$$

where for any $k \in \{0,\dots,n-1\}$, the inner optimization is over $(n_1,\dots,n_{k+1}) \in (\mathbb{N}^+)^{k+1}$, such that $\sum_{i=1}^{k+1} n_i = n$. Moreover, given $\mathbf{n} = (n_1,\dots,n_{k+1})$, $\sum_{j=1}^{k+1} n_j = n$, for any $j \in \{1,\dots,k+1\}$,

$$\mathcal{I}_j(\mathbf{n}) = \{\sum_{i=1}^{j-1} n_i + 1, \dots, \sum_{i=1}^{j} n_i\}. \tag{7}$$

Moreover, for $i \in \mathcal{I}_j$,

$$\hat{X}_i^{(2,b)} = \sqrt{\frac{1}{n_j}\sum_{l\in\mathcal{I}_j} Y_l^2}. \tag{8}$$

In other words, Lemma 1 implies that solving the BD-QMAP algorithm is equivalent to identifying the locations of the jumps such that, over each constant interval, the source input is estimated through appropriate averaging of the noisy observations, thereby minimizing the corresponding loss function. It is important to emphasize that if the regularization term enforcing the source structure were absent (i.e., if $\lambda = 0$), the concavity of the log function would result in the solution equaling the absolute value of input noisy sequence, with the maximal number of jumps. On the other hand, choosing λ too larges, will ensure that the output has no jumps.

The following theorem characterizes a lower bound on the performance achievable by BD-QMAP optimization (5).

Theorem 1. *Consider X^n generated by a stationary first-order Markov source $\mathbf{X} = \{X_i\}_{i\geq 1}$, characterized by $p(X_{i+1} = x_{i+1}|X_i = x_i) = (1-q_0)\delta_{x_i} + q_0\pi_c(x_m, x_M)$, where π_c denotes the pdf of an absolutely continuous distribution with bounded support $[x_m, x_M]$, $x_m > 0$. Let $\mathrm{E}[X_i^2] = \eta^2$. Let $\hat{X}^n$ denote the solution of BD-QMAP optimization, when the number of jumps are known to be $k = k(n)$. Then,*

$$\begin{aligned}\mathrm{E}[\frac{1}{n}\|X^n - \hat{X}^n\|_2^2] \geq & 2q_0\eta^2(q_0(3-\sqrt{2/\pi}-\sqrt{2\pi}) - q_0^2(2-\sqrt{2\pi}) + \mathrm{E}[T(1-\frac{1}{\sqrt{\mathrm{e}}}\frac{(1-\frac{1}{T})^{\frac{T}{2}}}{(1-\frac{2}{T})^{\frac{T-1}{2}}})\mathbb{1}_{T\geq 3}]) \\ & - 2M^2\Big(\frac{\epsilon}{1-\epsilon} + nq_0\mathrm{e}^{-\lfloor nq_0(1+\epsilon)\rfloor\left(q_0t_1+\ln\frac{1}{1+q_0t_1}\right)} + nq_0\mathrm{e}^{-\lfloor nq_0(1-\epsilon)\rfloor\left(q_0t_2+\ln\frac{1}{1+q_0t_2}\right)}\Big),\end{aligned}$$

where $T \sim \text{Geometric}(q_0)$ is representing the constant interval lengthes in the source.

Corollary 1. *Consider the same setup as in Theorem 1. Then,*

$$\mathrm{E}[\frac{1}{n}\|X^n - \hat{X}^n\|_2^2] \geq 2q_0\eta^2(q_0(3-\sqrt{2/\pi}-\sqrt{2\pi}) - q_0^2(2-\sqrt{2\pi}) + \mathrm{E}[T(1-\frac{1}{\sqrt{\mathrm{e}}}\frac{(1-\frac{1}{T})^{\frac{T}{2}}}{(1-\frac{2}{T})^{\frac{T-1}{2}}})\mathbb{1}_{T\geq 3}]) + \upsilon_n,$$

where $\upsilon_n = O(n^{-1/4})$.

4 Proofs

The following lemma will be used in the proof of the Theorem 1.

Lemma 2 (Concentration of Geometric [30])**.** *Let* $T_i \overset{iid}{\sim} \text{Geometric}(q_0) \quad \forall i \in \{1,\dots,N\}$ *, then for any* $t > 0$

$$P\left(\left|\frac{\sum_{i=1}^N T_i}{N} - \frac{1}{q_0}\right| > t\right) \leq 2e^{-N\left(q_0 t + \ln\frac{1}{1+q_0 t}\right)}.$$

Proof of Lemma 1. Note that the set $\mathcal{U}^n$ can be partitioned into n subsets depending on the number of jumps. That is, $\mathcal{U}^n = \bigcup_{i=0}^{n-1}\mathcal{U}_k$, where, for $k = 0,\dots,n-1$,

$$\mathcal{U}_k = \{u^n \in \mathcal{U}^n : \sum_{i=2}^n \mathbb{1}_{u_i \neq u_{i-1}} = k\}.$$

Then, the optimization in (5) can also be solved as follows

$$\begin{aligned}
&\min_{k\in\{0,\dots,n-1\}} \min_{u^n\in\mathcal{U}_k} [\frac{1}{n}\sum_{j=1}^n(\log u_i^2 + \frac{Y_i^2}{u_i^2}) + \frac{1}{n-1}(\lambda + \frac{1}{b}\eta)\sum_{i=2}^n \mathbb{1}_{u_i\neq u_{i-1}}] \\
&\equiv \min_{k\in\{0,\dots,n-1\}} \Big(\min_{u^n\in\mathcal{U}_k}\sum_{j=1}^n\big(\log u_i^2 + \frac{Y_i^2}{u_i^2}\big) + \frac{n}{n-1}(\lambda+\frac{1}{b})k\Big). \qquad (9)
\end{aligned}$$

First, consider the inner optimization which is over all sequences with exactly k jumps:

$$\min_{u^n\in\mathcal{U}_k}\big(\log u_i^2 + \frac{Y_i^2}{u_i^2}\big).$$

Consider a sequence with constant intervals of length $n_1,\dots,n_{k+1}$ with corresponding values $a_1,\dots,a_{k+1}$. (Clearly $\sum_{i=1}^{k+1} n_i = n$.) That is, u^n with k jumps is written as

$$u^n = \underbrace{a_1,\dots,a_1}_{n_1},\underbrace{a_2,\dots,a_2}_{n_2},\dots,\underbrace{a_{k+1},\dots,a_{k+1}}_{n_{k+1}}.$$

Then, the optimization can be written as

$$\min_{(n_1,\dots,n_{k+1}),(a_1,\dots,a_{k+1})\in\mathcal{U}^{k+1}}\big(\sum_{j=1}^{k+1}(n_j\log a_i^2 + \frac{1}{a_j^2}\sum_{l\in\mathcal{I}_j}Y_l^2)\big). \qquad (10)$$

where $\mathcal{I}_j$ is defined as (7). Then, it is easy to see that fixing the intervals, the optimal values can be found as

$$\hat{a}_j^2 = \frac{1}{n_j}\sum_{l\in\mathcal{I}_j}Y_l^2.$$

Using this observation, the optimization in (10) can be written as

$$\min_{(n_1,\ldots,n_{k+1})} \sum_{j=1}^{k+1} n_j \log\big(\frac{1}{n_j}\sum_{l\in\mathcal{I}_j} Y_l^2\big), \tag{11}$$

which yields the desired result. □

Proof of Theorem 1. Assuming that X^n contains $k = k(n)$ jumps, it can be written as

$$X^n = \underbrace{\alpha_1,\ldots,\alpha_1}_{T_1},\underbrace{\alpha_2,\ldots,\alpha_2}_{T_2},\ldots,\underbrace{\alpha_{k+1},\ldots,\alpha_{k+1}}_{T_{k+1}}.$$

Moreover, when the number of jumps (k) is known apriori by the algorithm, (6) simplifies to

$$\hat{X}^n = \min_{(n_1,\ldots,n_{k+1}):\,\sum_{i=1}^{k+1} n_i = n} \sum_{j=1}^{k+1} n_j \log\big(\frac{1}{n_j}\sum_{l\in\mathcal{I}_j} Y_l^2\big). \tag{12}$$

Clearly, the expected error is minimized when the locations of the jumps are detected correctly (i.e., $n_i = T_i$, $i = 1,\ldots,n+1$). We refer to this solution as the maximum likelihood (ML) solution, as it coincides with the ML solution when the number of jumps and their locations are known. As we just argued,

$$\mathrm{E}[\frac{1}{n}\|X^n - \hat{X}^n\|_2^2] \geq \mathrm{E}[\frac{1}{n}\|X^n - \hat{X}^{n,(\mathrm{ML})}\|_2^2].$$

For $j = 1,\ldots,k(n)+1$, define

$$\hat{\alpha}_j = \sqrt{\frac{1}{T_j}\sum_{l\in\mathcal{I}_j} Y_l^2} = \alpha_j\sqrt{\frac{1}{T_j}\sum_{l\in\mathcal{I}_j} W_l^2}. \tag{13}$$

Then, for $i \in \mathcal{I}_j$,

$$\hat{X}_i^{(\mathrm{ML})} = \hat{\alpha}_j, \tag{14}$$

which implies that

$$\begin{aligned}
\frac{1}{n}\|X^n - \hat{X}^{n,(\mathrm{ML})}\|_2^2 &= \frac{1}{n}\sum_{j=1}^{k}\alpha_j^2 T_j\left(1-\sqrt{\frac{1}{T_j}\sum_{l\in\mathcal{I}_j} W_l^2}\right)^2 + T_{k+1}\frac{\alpha_{k+1}^2}{n}\left(1-\sqrt{\frac{1}{T_{k+1}}\sum_{l\in\mathcal{I}_{k+1}} W_l^2}\right)^2 \\
&\geq \frac{1}{n}\sum_{j=1}^{k}\alpha_j^2 T_j\left(1-\sqrt{\frac{1}{T_j}\sum_{l\in\mathcal{I}_j} W_l^2}\right)^2 \\
&= \frac{q_0}{k}\sum_{j=1}^{k}\alpha_j^2 T_j\left(1-\sqrt{\frac{1}{T_j}\sum_{l\in\mathcal{I}_j} W_l^2}\right)^2 + (\frac{k}{n}-q_0)\frac{1}{k}\sum_{j=1}^{k}\alpha_j^2 T_j\left(1-\sqrt{\frac{1}{T_j}\sum_{l\in\mathcal{I}_j} W_l^2}\right)^2 \\
&\overset{(a)}{\geq} \frac{q_0}{k}\sum_{j=1}^{k}\alpha_j^2 T_j\left(1-\sqrt{\frac{1}{T_j}\sum_{l\in\mathcal{I}_j} W_l^2}\right)^2 - |\frac{k}{n}-q_0|\frac{M^2}{k}\sum_{j=1}^{k} T_j(1+\frac{1}{T_j}\sum_{l\in\mathcal{I}_j} W_l^2)
\end{aligned}$$

$$\overset{\text{(b)}}{\geq} \frac{q_0}{k}\sum_{j=1}^{k}\alpha_j^2 T_j\left(1-\sqrt{\frac{1}{T_j}\sum_{l\in\mathcal{I}_j}W_l^2}\right)^2 - |\frac{1}{q_0}-\frac{n}{k}|M^2 q_0(1+\frac{1}{n}\sum_{l=1}^{n}W_l^2), \tag{15}$$

where (a) follows because $(a-b)^2 \leq a^2+b^2$ for all a, b and (b) holds because $\sum_{j=1}^{k} T_j \leq n$ and $\sum_{j=1}^{k}\sum_{l\in\mathcal{I}_j} W_l^2 \leq \sum_{l=1}^{n} W_l^2$.

Taking the expected value of both sides of (15), it follows that

$$\begin{aligned}
\mathrm{E}[\frac{1}{n}\|X^n-\hat{X}^{n,(\mathrm{ML})}\|_2^2] &\geq q_0\eta^2\,\mathrm{E}\left[T\Big(1-\sqrt{\frac{1}{T}\sum_{i=1}^{T}W_i^2}\,\Big)^2\right] - M^2 q_0\,\mathrm{E}\left[|\frac{1}{q_0}-\frac{n}{k}|(1+\frac{1}{n}\sum_{l=1}^{n}W_l^2)\right] \\
&= q_0\eta^2\,\mathrm{E}\left[T\Big(1-\sqrt{\frac{1}{T}\sum_{i=1}^{T}W_i^2}\,\Big)^2\right] - 2M^2 q_0\,\mathrm{E}\left[|\frac{1}{q_0}-\frac{n}{k}|\right],
\end{aligned} \tag{16}$$

where the last line follows because the source $\mathbb{X}$ and the speckle noise process are independent. We first focus on the first term. Note that

$$\begin{aligned}
\mathrm{E}\left[T\Big(1-\sqrt{\frac{1}{T}\sum_{j=1}^{T}w_j^2}\,\Big)^2\right] &= \mathrm{E}\left[T\Big(1+\frac{1}{T}\sum_{j=1}^{T}w_j^2-2\sqrt{\frac{1}{T_i}\sum_{j=1}^{T_i}w_j^2}\Big)\right] \\
&= \mathrm{E}\left[2T-2T\sqrt{\frac{1}{T}\sum_{j=1}^{T}w_j^2}\,\right] \\
&= 2\,\mathrm{E}\left[T-\sqrt{2T}\frac{\Gamma(\frac{T+1}{2})}{\Gamma(\frac{T}{2})}\right],
\end{aligned} \tag{17}$$

where the last line follows because

$$\mathrm{E}\left[\sqrt{T\sum_{j=1}^{T}w_j^2}\,\right] = \mathrm{E}\left[\mathrm{E}\left[\sqrt{T\sum_{j=1}^{T}w_j^2}\,\middle|\,T\right]\right] = \mathrm{E}\left[\sqrt{2T}\frac{\Gamma(\frac{T+1}{2})}{\Gamma(\frac{T}{2})}\right]. \tag{18}$$

It can be shown that, for all $x>0$,

$$\sqrt{2\pi}x^{x+0.5}\mathrm{e}^{-x}\mathrm{e}^{\frac{1}{1+12x}} \leq \Gamma(x+1) \leq \sqrt{2\pi}x^{x+0.5}\mathrm{e}^{-x}\mathrm{e}^{\frac{1}{12x}}. \tag{19}$$

Therefore, for $T>2$,

$$\begin{aligned}
\frac{\Gamma(\frac{T+1}{2})}{\Gamma(\frac{T}{2})} &\leq \frac{(\frac{T-1}{2})^{\frac{T}{2}}\mathrm{e}^{-(T-1)/2}\mathrm{e}^{\frac{1}{6(T-1)}}}{(\frac{T}{2}-1)^{\frac{T-1}{2}}\mathrm{e}^{-T/2+1}\mathrm{e}^{\frac{1}{6T-11}}} \\
&= \mathrm{e}^{-\frac{1}{2}}\sqrt{\frac{T}{2}}(1-\frac{1}{T})^{\frac{T}{2}}(1-\frac{2}{T})^{-\frac{T-1}{2}}\mathrm{e}^{\frac{1}{6(T-1)}-\frac{1}{6T-11}} \\
&= \mathrm{e}^{-\frac{1}{2}}\sqrt{\frac{T}{2}}\exp\Big(\frac{T}{2}\ln(1-\frac{1}{T})-\frac{T-1}{2}\ln(1-\frac{2}{T})+\frac{1}{6(T-1)}-\frac{1}{6T-11}\Big) \\
&\leq \mathrm{e}^{-\frac{1}{2}}\sqrt{\frac{T}{2}}\exp\Big(\frac{T}{2}\ln(1-\frac{1}{T})-\frac{T-1}{2}\ln(1-\frac{2}{T})\Big) \\
&= \sqrt{\frac{T}{2\mathrm{e}}}\frac{(1-\frac{1}{T})^{\frac{T}{2}}}{(1-\frac{2}{T})^{\frac{T-1}{2}}}.
\end{aligned} \tag{20}$$

Therefore, we can bound (17) as

$$2\,\mathrm{E}\left[T-\sqrt{2T}\frac{\Gamma(\frac{T+1}{2})}{\Gamma(\frac{T}{2})}\right]\geq 2q_0(1-\frac{\sqrt{2}}{\Gamma(0.5)})+2q_0(1-q_0)(2-2\Gamma(1.5))+2\,\mathrm{E}[T(1-\frac{1}{\sqrt{\mathrm{e}}}\frac{(1-\frac{1}{T})^{\frac{T}{2}}}{(1-\frac{2}{T})^{\frac{T-1}{2}}})\mathbb{1}_{T\geq 3}] \tag{21}$$

Combining (16) and (21), it follows that

$$\mathrm{E}[\frac{1}{n}\|X^n-\hat{X}^{n,(\mathrm{ML})}\|_2^2]\geq q_0\eta^2(2q_0(1-\frac{\sqrt{2}}{\Gamma(0.5)})+2q_0(1-q_0)(2-2\Gamma(1.5)) \tag{22}$$

$$+\,2\,\mathrm{E}[T(1-\frac{1}{\sqrt{\mathrm{e}}}\frac{(1-\frac{1}{T})^{\frac{T}{2}}}{(1-\frac{2}{T})^{\frac{T-1}{2}}})\mathbb{1}_{T\geq 3}])-2M^2q_0\,\mathrm{E}\left[|\frac{1}{q_0}-\frac{n}{k}|\right]. \tag{23}$$

To bound the last term, note that k is a random variable that depends on n. Given $\epsilon>0$, define event $\mathcal{E}$ as

$$\mathcal{E}=\{nq_0(1-\epsilon)\leq k(n)\leq nq_0(1+\epsilon)\}. \tag{24}$$

Note that conditioned on $\mathcal{E}$, we have $1-\epsilon\leq\frac{k(n)}{nq_0}\leq 1+\epsilon$, which implies that

$$\frac{1}{q_0(1+\epsilon)}-\frac{1}{q_0}\leq\frac{n}{k}-\frac{1}{q_0}\leq\frac{1}{q_0(1-\epsilon)}-\frac{1}{q_0}.$$

Using this observation, we can bound the remaining term in (23), as follows:

$$\begin{aligned}\mathrm{E}\left[|\frac{1}{q_0}-\frac{n}{k}|\right]&=\mathrm{E}\left[|\frac{1}{q_0}-\frac{n}{k}|(\mathbb{1}_{\mathcal{E}}+\mathbb{1}_{\mathcal{E}^c})\right]\\&\leq\frac{\epsilon}{q_o(1-\epsilon)}+nP(\mathcal{E}^c).\end{aligned} \tag{25}$$

Finally, to bound $P(\mathcal{E}^c)$, note that

$$\begin{aligned}P(k(n)\geq nq_0(1+\epsilon))&=P(\sum_{i=1}^{\lfloor nq_0(1+\epsilon)\rfloor}T_i<n)\\&=P\left(\frac{1}{\lfloor nq_0(1+\epsilon)\rfloor}\sum_{i=1}^{\lfloor nq_0(1+\epsilon)\rfloor}T_i-\frac{1}{q_0}<\frac{n}{\lfloor nq_0(1+\epsilon)\rfloor}-\frac{1}{q_0}\right)\\&\leq P\left(|\frac{1}{q_0}-\frac{1}{\lfloor nq_0(1+\epsilon)\rfloor}\sum_{i=1}^{\lfloor nq_0(1+\epsilon)\rfloor}T_i|>\frac{1}{q_0}-\frac{n}{\lfloor nq_0(1+\epsilon)\rfloor}\right)\\&\leq\mathrm{e}^{-\lfloor nq_0(1+\epsilon)\rfloor\left(q_0t_1+\ln\frac{1}{1+q_0t_1}\right)},\end{aligned} \tag{26}$$

where the last line follows from Lemma 2, with

$$t_1=\frac{1}{q_0}-\frac{n}{\lfloor nq_0(1+\epsilon)\rfloor}.$$

Similarly, again using Lemma 2, we have

$$P(k(n)\leq nq_0(1-\epsilon))=P(\sum_{i=1}^{\lfloor nq_0(1-\epsilon)\rfloor}T_i>n)$$

$$= P\Big(\frac{1}{\lfloor nq_0(1-\epsilon)\rfloor}\sum_{i=1}^{\lfloor nq_0(1-\epsilon)\rfloor} T_i - \frac{1}{q_0} > \frac{n}{\lfloor nq_0(1-\epsilon)\rfloor} - \frac{1}{q_0}\Big)$$
$$\leq \mathrm{e}^{-\lfloor nq_0(1-\epsilon)\rfloor\left(q_0t_2+\ln\frac{1}{1+q_0t_2}\right)}, \tag{27}$$

with

$$t_2 = \frac{n}{\lfloor nq_0(1-\epsilon)\rfloor} - \frac{1}{q_0}.$$

Combining (25), (26) and (27) with (23) yields the desired result. That is,

$$\mathrm{E}[\frac{1}{n}\|X^n - \hat{X}^n\|_2^2] \geq q_0\eta^2(2q_0(1-\frac{\sqrt{2}}{\Gamma(0.5)}) + 2q_0(1-q_0)(2-2\Gamma(1.5)) + 2\,\mathrm{E}[T(1-\frac{1}{\sqrt{\mathrm{e}}}\frac{(1-\frac{1}{T})^{\frac{T}{2}}}{(1-\frac{2}{T})^{\frac{T-1}{2}}})\mathbb{1}_{T\geq 3}]) \tag{28}$$
$$- 2M^2q_0\Big(\frac{\epsilon}{q_o(1-\epsilon)} + n\mathrm{e}^{-\lfloor nq_0(1+\epsilon)\rfloor\left(q_0t_1+\ln\frac{1}{1+q_0t_1}\right)} + n\mathrm{e}^{-\lfloor nq_0(1-\epsilon)\rfloor\left(q_0t_2+\ln\frac{1}{1+q_0t_2}\right)}\Big). \tag{29}$$

□

Proof of Corollary 1. For $x \geq 0$ we can show [31] that $\ln(1+x) \leq x\frac{x+6}{2x+6}$ thus,

$$x - \ln(1+x) \geq \frac{x^2}{2x+6}. \tag{30}$$

In addition, we have

$$1 - \frac{x}{\lfloor x(1+x^{-1/4})\rfloor} = \Omega(\frac{1}{x^{1/3}}), \tag{31}$$

and,

$$\frac{x}{\lfloor x(1-x^{-1/4})\rfloor} - 1 = \Omega(\frac{1}{x^{1/3}}). \tag{32}$$

(31) holds for $x \geq x_0$,

$$\begin{aligned}
1 - \frac{x}{\lfloor x+x^{3/4}\rfloor} &= 1 - \frac{x}{\lfloor x+x^{3/4}\rfloor - x - x^{3/4} + x + x^{3/4}} \\
&\geq 1 - \frac{x}{-1+x+x^{3/4}} \\
&= \frac{x^{3/4}-1}{x+x^{3/4}-1} \\
&= \frac{1}{x^{1/3}}\underbrace{\left(\frac{x^{3/4}-1}{x^{2/3}+x^{5/12}-x^{-1/3}}\right)}_{(*)} \\
&\geq \frac{1}{x^{1/3}},
\end{aligned}$$

where x_0 is some point after which $(*)$ remains greater than one. Similar steps proves (32).

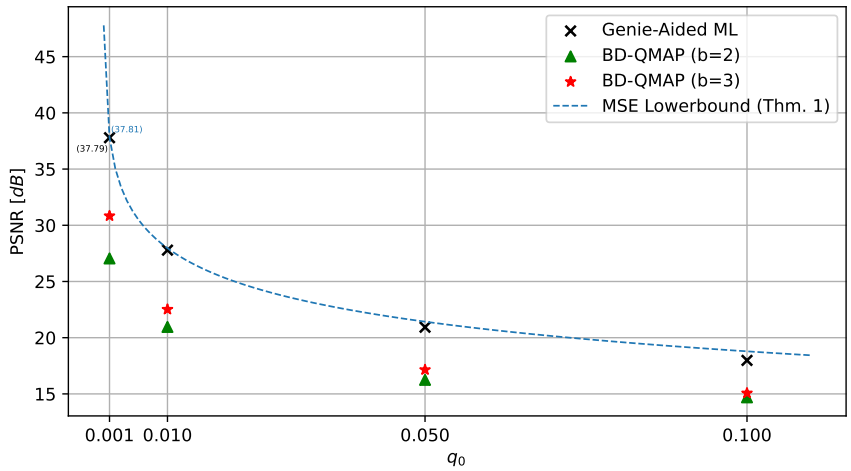

Figure 1: MSE lower bound of the genie-aided ML despeckler as derived in Theorem 1 and the proposed BD-QMAP despecker for piecewise constant source with parameter q_0. ($\text{PSNR} = 10\log_{10}(\text{MAX}^2 / \text{MSE})$ where MAX is the maximum value of signal's support set)

Let $\epsilon = (nq_0)^{-1/4}$ in the result of Theorem 1, using (31), (32) we have $q_0 t_1 = \Omega(n^{-1/3})$ and $q_0 t_2 = \Omega(n^{-1/3})$, and applying (30) we have

$$\begin{aligned}\mathrm{E}[\frac{1}{n}\|X^n - \hat{X}^n\|_2^2] \geq & q_0\eta^2(2q_0(1-\frac{\sqrt{2}}{\Gamma(0.5)}) + 2q_0(1-q_0)(2-2\Gamma(1.5)) + 2\,\mathrm{E}[T(1-\frac{1}{\sqrt{\mathrm{e}}}\frac{(1-\frac{1}{T})^{\frac{T}{2}}}{(1-\frac{2}{T})^{\frac{T-1}{2}}})\mathbb{1}_{T\geq 3}]) \\ & - 2M^2\Big(\frac{(nq_0)^{-1/4}}{1-(nq_0)^{-1/4}} + q_0 n\mathrm{e}^{-\lfloor nq_0(1+(nq_0)^{\frac{-1}{4}})\rfloor\left(\frac{c_1^2 n^{\frac{-2}{3}}}{2n^{\frac{-1}{3}}+6}\right)} + q_0 n\mathrm{e}^{-\lfloor nq_0(1-(nq_0)^{\frac{-1}{4}})\rfloor\left(\frac{c_2^2 n^{\frac{-2}{3}}}{2n^{\frac{-1}{3}}+6}\right)}\Big),\end{aligned}$$

where $c_1, c_2 \in \mathbb{R}^+$ are constants. Second line converges to zero as $n \to \infty$ with $O(n^{-1/4})$. □

5 Numerical experiments

In the following, we first address the practical implementation of the BD-QMAP optimization problem. We then compare the performance of BD-QMAP with the lower bound derived in Theorem 1. Finally, we perform comparative studies on despeckling for piecewise-constant sources and extending the BD-QMAP to be applied on high dimensional images.

5.1 Algorithmic considerations

As noted in Remark 1, addressing the distinct search spaces of the log-likelihood and regularizer in BD-QMAP is essential for practical implementation, and limiting the search to the quantized space ensures feasibility. This restriction enables the discrete suboptimal optimization to be efficiently performed using the Viterbi algorithm [32]. Therefore, to tackle the optimization problem of BD-QMAP, we begin by limiting the search space in (3) to b-bit quantized realizations, denoted as $\mathcal{X}_b^n$. We call this suboptimal despeckler BD-QMAP$_b$, as it is optimizing the both terms of (3) in the b-bit quantized space. In other words, BD-QMAP$_b$ solves the following optimization

$$\arg\min_{u^n \in \mathcal{X}_b^n} \frac{1}{n}\sum_{i=k}^{n}(\log u_i^2 + \frac{y_i^2}{u_i^2} + \frac{\lambda}{b} w_{u_{i-k+1}^i}), \tag{33}$$

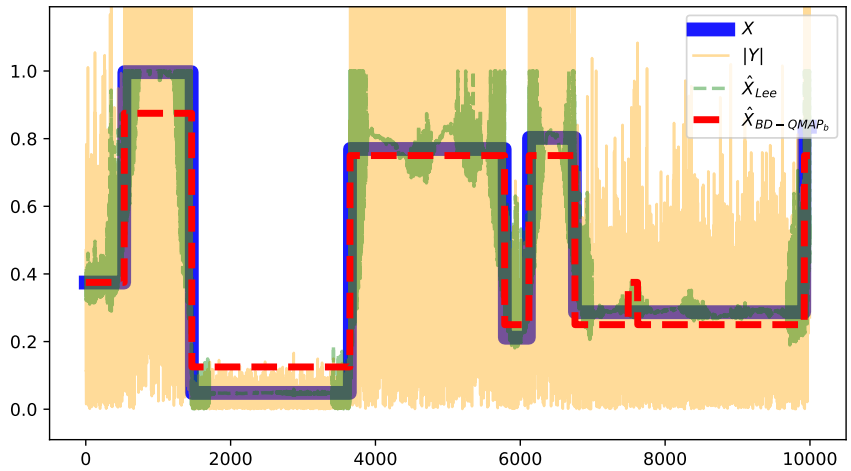

Figure 2: Piecewise constant source (X) with parameter $q_0 = 0.001$ sampled under speckle noise (Y), enhanced Lee and BD-QMAP$_b$ despeckled reconstructions, as discussed in Section 5.

where $c_{\mathbf{w}}(u^n)$ is scaled by $(n-k+1)/n$ without an impact on the optimal solution as it can be absorbed in the hyper-parameter λ. Since similar to the the additive case, the negative log likelihood function of u^n is the sum of n element-wise distinct functions, with the i-th function only depending on u_i, the Viterbi algorithm [32] can still be employed to solve (33).

The Viterbi algorithm operates on a trellis diagram with n stages, each having $|\mathcal{X}_b|^k$ states. State s_i in the diagram corresponds to the subsequence u_{i-k+1}^i of length k in the candidate solution. Let the cost associated to the state $s_i = u_{i-k+1}^i$ in the diagram follows the recursive rule as,

$$C_i(s_i) = \min_{s' \in \mathcal{S}(s_i)} (\log u_i^2 + \frac{y_i^2}{u_i^2} + \frac{\lambda}{b} w_{u_{i-k+1}^i}) + C_{i-1}(s'),$$

for any $i \in \{k, \ldots, n\}$, where $\mathcal{S}(s_i)$ denotes the set of all closest states that transition into the state s_i and $|\mathcal{S}(s_i)| = |\mathcal{X}_b|$. The state $s' = u_{i-k}^{i-1}$ represents the previous state leading to s_i. Thus BD-QMAP$_b$ solution can be found recursively starting minimizing $C_n(s_n)$.

5.2 Theoretical lower bound

In Theorem 1, a lower bound on the best achievable reconstruction error was derived for the piecewise constant source. To explore this bound in practice, we compare it to an ideal despeckler for piecewise constant sources, referred to as the *genie-aided maximum likelihood (ML)* despeckler. This estimator has access to the exact jump locations in the ground truth data in addition to the noisy observations. With such side information, the reconstruction error is minimized using Equation (8) for each constant segment between consecutive jump locations. For comparison, we evaluated the performance of this genie-aided despeckler against BD-QMAP. The BD-QMAP implementation, as detailed in Section 5.3.1, was applied to piecewise constant sources with $q_0 \in \{0.001, 0.01, 0.05, 0.1\}$. Each data point in the figure represents the average error over a test set of 100 realizations with fixed q_0, each of length $n = 10^6$.

5.3 Comparative analysis of despeckling for piecewise constant sources

For numerical experiments with the piecewise constant source introduced in Section 3.2 we assume the absolute continous distribution to be uniform on the interval $[0, 1]$. A sample realization of this source under

speckle noise is shown in Figure 2. Considering this source, the pivotal parameter which directly affects the performance of the despeckler is q_0, i.e., the probability of signal level-change which also determines the level of structure for the analog source [29]. To learn the weights of the Equation (2) to be used in the regularizer term of the BD-QMAP loss function, for a fixed q_0, we sample the random process for 10^7 points and find the empirical second order distribution by counting the occurances of the b bit quantized samples of length two. Key advantages of BD-QMAP over other despecklers in the literature in practice are two fold. First, the BD-QMAP assumes no upperbound on the speckle power level on the observation as opposed to [13,14], and also [8] in which the filter is bypassed completely in high noise level regimes. Second, the BD-QMAP method is applicable to any given source without requiring restrictive assumptions on the signal's prior distribution. This flexibility contrasts with the strong assumptions imposed by other Bayesian filters, such as those in [6,7,10]. Each entry in the Table 1 is the despeckling performance for a test dataset of size 100 of piecewise constant signals of length $n = 10^6$.

5.3.1 BD-QMAP implementation

Using the Viterbi implementation described in Section 5.1 for $k = 2$, we can efficiently implement BD-QMAP$_b$. As noted in Remark 1, the fidelity term in BD-QMAP optimization is not restricted to a quantized space. Therefore, to enhance the BD-QMAP$_b$ solution, we refine it by identifying the detected jump locations and computing the ML estimates on the intervals between them using Equation (8). This refinement significantly improves performance, especially for highly structured sources (i.e., when q_0 is small). As shown in Table 1, the despeckling performance of BD-QMAP$_b$ for highly structured sources improves substantially when the initial estimate is refined for the final BD-QMAP solution. Notably, even a low-complexity implementation with $b = 2$ is effective in detecting jump locations, with the refinement step yielding significant gains.

5.3.2 Regularization and quantization in BD-QMAP

To explore the effectiveness of the regularizer of the BD-QMAP in finding the structure of the source, and yeilding lower errors, we conducted experiments for a range of values for λ in Equation (3), as shown in Figure 3. It can be seen that when $\lambda = 0$ the despeckler is not able to distinguish between different levels of structuredness (as measured by q_0), however a small regularization would let the denoiser to recover the empirical distribution of the ground-truth distribution in the reconstruction. Finally, as expected, a large value of λ would decrease the fidelity of the reconstruction to the observed noisy signal. The number of bits used to quantize the source for the learned weights significantly impacts both the final performance and the time complexity of the optimization problem in Equation (3), as the size of the search space increases exponentially with the number of bits.

In general, achieving better reconstruction results necessitates selecting the number of bits b in BD-QMAP as high as computationally feasible. However, for highly structured data (e.g., high-resolution images), a relatively small number of bits can suffice to uncover the structure of the source from noisy observations. As demonstrated in Figure 3, when $q_0 = 0.001$ (indicating a highly structured source), the suboptimal solution of BD-QMAP$_b$ with just 2 bits effectively captures the source structure. Upon refining the solution to account for quantization error, it achieves a higher PSNR than BD-QMAP$_b$ with 3 bits. This experiment suggests that for highly structured sources, selecting fewer bits is often sufficient to match the distribution, avoiding the computational challenges associated with higher bit counts.

5.3.3 Linear adaptive filters

All the linear adaptive filters in Table 1 require a window size hyper-parameter that defines the area over which the local statistics will be calculated. In these experiments this value is set to $1/2q_0$, half of the expected interval lengths of constant pieces in the source.

We also conduct experiments with an *Enhanced* version of the filters which is based on the idea of thresholding

Table 1: Despeckling Performance Comparison (PSNR) for Piecewise Constant Source.

	$q_0 = 0.1$	$q_0 = 0.01$	$q_0 = 0.001$
Speckled Source	8.710	8.742	9.055
Box Car Filter	13.226	16.321	16.976
Frost Filter [33]	12.923	13.900	14.226
Total Variation [14]	9.339	10.895	11.483
Lee Filter [6] / Enhanced [8]	10.505 / 13.865	18.402 / 19.703	22.303 / 22.577
Kuan Filter [7] / Enhanced [8]	11.618 / 14.041	19.650 / 20.375	23.017 / 23.244
BD-QMAP$_b$ (b=2 / b=3)	14.786 / 15.478	17.909 / 21.613	19.530 / 24.363
BD-QMAP (b=2 / b=3)	14.696 / 15.072	20.961 / 22.518	27.052 / 30.831

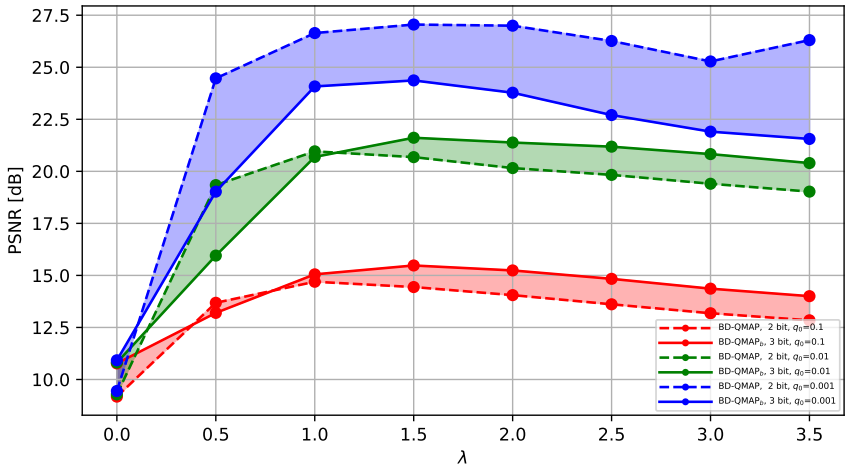

Figure 3: Effect of hyperparameter λ in BD-QMAP$_b$ and BD-QMAP optimization for different choices of bits (b) and source structure (q_0).

local variance, as suggested in [8]. To improve the final performance of the filters, three statiscical classes are considered which are known as *heterogeneity adjustments* in the literature. The simple modification is to distinguish between three region of operation: homogeneous, heterogenous, and strongly speckled. To decide in which region the filter operates, if the observation variation coefficient defined as $C_Y \triangleq \frac{\mathrm{Var}(Y)}{\mathrm{E}[Y]}$ of the local window falls below a threshold of noise variation coefficient, similarly defined to be $C_W \triangleq \frac{\mathrm{Var}(W)}{\mathrm{E}[W]}$, we only do keep the mean window mean value as the despeckled pixel. On the other hand, if $C_Y \geq C_{\max}$, the filter output is bypassed and the despeckled pixel is equal to the speckled observed pixel, where empirically the optimal value of $C_{\max}$ is set to $\sqrt{3}C_W$ [8]. The *Enhanced* version of the filters mentioned in Table 1 refer to applying the filter only when $C_W \leq C_Y \leq C_{\max}$.

6 Conclusion

A novel Bayesian despeckling method is proposed for structured sources. Its performance is analyzed for piecewise constant structured sources, and a lower bound on the minimum achievable MSE is derived. The results demonstrate that the despeckler effectively detects edges under speckle noise, achieving superior performance compared to other theoretically grounded approaches.

Acknowledgment

AZ and SJ were supported by NSF grant CCF-2237538.

References

[1] F. Argenti, A. Lapini, T. Bianchi, and L. Alparone, "A tutorial on speckle reduction in synthetic aperture radar images," *IEEE Geoscience and Remote Sensing Magazine*, vol. 1, no. 3, pp. 6–35, 2013. 1

[2] V. Bianco, P. Memmolo, M. Leo, S. Montresor, C. Distante, M. Paturzo, P. Picart, B. Javidi, and P. Ferraro, "Strategies for reducing speckle noise in digital holography," *Light: Science & Applications*, vol. 7, no. 1, p. 48, 2018. 1

[3] J. M. Schmitt, S. Xiang, and K. M. Yung, "Speckle in optical coherence tomography," *Journal of biomedical optics*, vol. 4, no. 1, pp. 95–105, 1999. 1

[4] R. Touzi, "A review of speckle filtering in the context of estimation theory," *IEEE Transactions on Geoscience and Remote Sensing*, vol. 40, no. 11, pp. 2392–2404, 2002. 1

[5] J. W. Goodman, *Speckle phenomena in optics: theory and applications*. Roberts and Company Publishers, 2007. 1

[6] J.-S. Lee, "Digital image enhancement and noise filtering by use of local statistics," *IEEE Transactions on Pattern Analysis and Machine Intelligence*, no. 2, pp. 165–168, 1980. 1, 13, 14

[7] D. T. Kuan, A. A. Sawchuk, T. C. Strand, and P. Chavel, "Adaptive noise smoothing filter for images with signal-dependent noise," *IEEE Transactions on Pattern Analysis and Machine Intelligence*, no. 2, pp. 165–177, 1985. 2, 13, 14

[8] A. Lopes, R. Touzi, and E. Nezry, "Adaptive speckle filters and scene heterogeneity," *IEEE transactions on Geoscience and Remote Sensing*, vol. 28, no. 6, pp. 992–1000, 1990. 2, 13, 14, 15

[9] J.-S. Lee, "Refined filtering of image noise using local statistics," *Computer graphics and image processing*, vol. 15, no. 4, pp. 380–389, 1981. 2

[10] A. Lopes, E. Nezry, R. Touzi, and H. Laur, "Maximum a posteriori speckle filtering and first order texture models in sar images," in *10th annual international symposium on geoscience and remote sensing*. Ieee, 1990, pp. 2409–2412. 2, 13

[11] D. Kuan, A. Sawchuk, T. Strand, and P. Chavel, "Adaptive restoration of images with speckle," *IEEE Transactions on Acoustics, Speech, and Signal Processing*, vol. 35, no. 3, pp. 373–383, 1987. 2

[12] L. I. Rudin, S. Osher, and E. Fatemi, "Nonlinear total variation based noise removal algorithms," *Physica D: nonlinear phenomena*, vol. 60, no. 1-4, pp. 259–268, 1992. 2

[13] G. Aubert and J.-F. Aujol, "A variational approach to removing multiplicative noise," *SIAM Journal on Applied Mathematics*, vol. 68, no. 4, pp. 925–946, 2008. 2, 13

[14] J. Shi and S. Osher, "A nonlinear inverse scale space method for a convex multiplicative noise model," *SIAM Journal on Imaging Sciences*, vol. 1, no. 3, pp. 294–321, 2008. 2, 13, 14

[15] C.-A. Deledalle, L. Denis, and F. Tupin, "Iterative weighted maximum likelihood denoising with probabilistic patch-based weights," *IEEE transactions on Image Processing*, vol. 18, no. 12, pp. 2661–2672, 2009. 2

[16] S. Parrilli, M. Poderico, C. V. Angelino, and L. Verdoliva, "A nonlocal sar image denoising algorithm based on llmmse wavelet shrinkage," *IEEE Transactions on Geoscience and Remote Sensing*, vol. 50, no. 2, pp. 606–616, 2011. 2

[17] X. X. Zhu, S. Montazeri, M. Ali, Y. Hua, Y. Wang, L. Mou, Y. Shi, F. Xu, and R. Bamler, "Deep learning meets SAR: Concepts, models, pitfalls, and perspectives," *IEEE Geoscience and Remote Sensing Magazine*, vol. 9, no. 4, pp. 143–172, 2021. 2

[18] K. Zhang, W. Zuo, Y. Chen, D. Meng, and L. Zhang, "Beyond a gaussian denoiser: Residual learning of deep cnn for image denoising," *IEEE transactions on image processing*, vol. 26, no. 7, pp. 3142–3155, 2017. 2

[19] G. Chierchia, D. Cozzolino, G. Poggi, and L. Verdoliva, "Sar image despeckling through convolutional neural networks," in *2017 IEEE international geoscience and remote sensing symposium (IGARSS)*. IEEE, 2017, pp. 5438–5441. 2

[20] P. Wang, H. Zhang, and V. M. Patel, "Sar image despeckling using a convolutional neural network," *IEEE Signal Processing Letters*, vol. 24, no. 12, pp. 1763–1767, 2017. 2

[21] J. Lehtinen, J. Munkberg, J. Hasselgren, S. Laine, T. Karras, M. Aittala, and T. Aila, "Noise2Noise: Learning image restoration without clean data," in *Proceedings of the 35th International Conference on Machine Learning*, vol. 80. PMLR, 2018, pp. 2965–2974. 2

[22] A. Krull, T.-O. Buchholz, and F. Jug, "Noise2void-learning denoising from single noisy images," in *Proceedings of the IEEE/CVF conference on computer vision and pattern recognition*, 2019, pp. 2129–2137. 2

[23] E. Dalsasso, L. Denis, and F. Tupin, "Sar2sar: A semi-supervised despeckling algorithm for sar images," *IEEE Journal of Selected Topics in Applied Earth Observations and Remote Sensing*, vol. 14, pp. 4321–4329, 2021. 2

[24] A. B. Molini, D. Valsesia, G. Fracastoro, and E. Magli, "Speckle2void: Deep self-supervised sar despeckling with blind-spot convolutional neural networks," *IEEE Transactions on Geoscience and Remote Sensing*, vol. 60, pp. 1–17, 2021. 2

[25] T. L. Bobrow, F. Mahmood, M. Inserni, and N. J. Durr, "Deeplsr: a deep learning approach for laser speckle reduction," *Biomedical optics express*, vol. 10, no. 6, pp. 2869–2882, 2019. 2

[26] S. Guha and S. T. Acton, "SDDPM: Speckle denoising diffusion probabilistic models," *arXiv preprint arXiv:2311.10868*, 2023. 2

[27] W. Zhou, J. Wabnig, and S. Jalali, "Bayesian denoising of structured sources and its implications on learning-based denoising," *Information and Inference: A Journal of the IMA*, vol. 12, no. 4, pp. 2503–2545, 2023. 2, 3, 4, 5

[28] Y. Wu and S. Verdú, "Rényi information dimension: Fundamental limits of almost lossless analog compression," *IEEE Transactions on Information Theory*, vol. 56, no. 8, pp. 3721–3748, 2010. 4

[29] S. Jalali and H. V. Poor, "Universal compressed sensing for almost lossless recovery," *IEEE Transactions on Information Theory*, vol. 63, no. 5, pp. 2933–2953, 2017. 4, 13

[30] S. Janson, "Tail bounds for sums of geometric and exponential variables," *Statistics & Probability Letters*, vol. 135, pp. 1–6, 2018. 6

[31] F. Topsøe, *Some Bounds for the Logarithmic Function.* United States: Nova Science Publishers, 2007, vol. 4, pp. 137–151. 10

[32] G. D. Forney, "The viterbi algorithm," *Proceedings of the IEEE*, vol. 61, no. 3, pp. 268–278, 1973. 11, 12

[33] V. S. Frost, J. A. Stiles, K. S. Shanmugan, and J. C. Holtzman, "A model for radar images and its application to adaptive digital filtering of multiplicative noise," *IEEE Transactions on Pattern Analysis and Machine Intelligence*, no. 2, pp. 157–166, 1982. 14